Master of Science Thesis

Temperature dependence of grain-scale slip behavior of muscovite and implications for subduction zone seismogenesis

Ronald Petrus Johannes Pijnenburg

March 2012

Faculty of Geosciences

Department of Earth Sciences

Utrecht University

Supervisors:

S.A.M. den Hartog, MSc and Prof. Dr. C.J. Spiers

Universiteit Utrecht

A cane non magno saepe tenetur aper

Ovidius, Remedia Amoris 422

A boar is often held by quite a small dog

Abstract

Despite extensive work on the frictional or plastic strength of muscovite gouge, little is known about grain-scale processes controlling muscovite sliding. In this study we perform direct shear experiments on two muscovite crystals, shearing them parallel to their interface formed by the (001) plane, at 150°, 500° and 600°C. We conducted pressure stepping tests (270 – 170 MPa) and velocity stepping tests (0.1-10 μm/s), to provide constraints on muscovite single crystal rheology. The crystallographic orientation of the crystals was controlled to either inhibit dislocation glide, (shear parallel to the [010] direction) or to enhance dislocation glide (shear parallel to the [100] direction). It is found that the strength of muscovite single crystals at these conditions is pressure sensitive (μ = 0.055 – 0.12), rate-dependent in a velocity strengthening sense and inclined to weaken with temperature. This illustrates a pronounced difference from sliding behavior reported in studies on muscovite gouge. Microstructural analysis implies dislocation glide to be strongly affected by temperature as well as shear direction, although more work seems needed to be conclusive on the mechanical implications of this. The friction coefficient for sliding on the (001) interface between the individual crystals tested, lies in the range of 0.055 (sliding in the [100] direction) to 0.12, (sliding in the [010] direction). It is tentatively concluded that muscovite single crystals, at the range of temperatures described in this study, consistently deform through a combination of crystal plastic and frictional processes, where strength is mostly controlled by grain boundary friction. Finally, it is noted that the frictional strength of muscovite single crystals might have previously been overestimated in studies on crustal strength. The present results might therefore have important implications for studies considering crustal strength and hence seismogenesis.

Table of contents

1) Introduction

In spite of the devastating effects of subduction megathrust earthquakes, the mechanisms of interplate seismogenesis remain poorly understood. It is now widely recognized that subduction megathrust seismogenesis is limited to the seismogenic zone (~150-350°C) that is bounded by regions of aseismic behavior (e.g. Scholz, 2002; Hyndman, 1997; 2007; Marone and Saffer, 2007). The location of these boundaries appears to be thermally controlled. While there is a general consensus that the downdip limit of interplate seismicity is controlled by either the onset of crystal plasticity at ~350° - 450°C (e.g. Scholz, 2002; Hyndman, 2007) or the intersection of the thrust with the fore-arc Moho (e.g. Peacock and Hyndman, 1999; Hyndman, 2007), there is little agreement regarding processes that control the updip limit of seismogenic faulting (figure 1).

It has been suggested by Marone and Scholz (1988) that the updip limit reflects a threshold lithification state within the fault gouge. These authors argue that unconsolidated gouge material above the seismogenic limit is characterized by distributed deformation, while deformation is localized in consolidated material. Since experimental studies show that brittle, localized deformation is related to stick-slip behavior whereas distributed deformation results in stable frictional sliding (Beeler et al., 1996; Marone, 1998; Scruggs and Tullis, 1998), the progressive consolidation of fault gouge may explain the onset of seismogenesis.

Alternatively, the coincidence of the temperature of the transition of the hydrous clay mineral smectite to anhydrous illite with that of the updip limit, has led to the suggestion that the presence of illite causes unstable behavior (Vrolijk, 1990). However, prerequisite for seismic behavior is that the frictional strength of a material decreases with increasing slip velocity, i.e. that the material exhibits velocity weakening behavior (Marone, 1998; Scholz, 2002; Marone and Saffer, 2007). Frictional experiments performed at room temperature however, has shown that although there is a difference in frictional strength between smectite and illite, the latter does not show velocity weakening behavior, making the dehydration of smectite a less likely candidate to account for the updip seismogenic limit (Marone and Saffer, 2007; Tembe et al., 2010).

The velocity dependence of friction is quantified by (e.g. Beeler et al., 1994, Marone, 1998 and Scholz, 2002):

$$(a-b) = \frac{\Delta\mu_{ss}}{\Delta ln\mathbf{V}} \qquad (1)$$

where $\Delta\mu_{ss}$ is a change in the steady state coefficient of friction μ, resulting from a stepwise change in slip velocity V. The parameter a represents the magnitude of instantaneous change in μ upon a change in sliding velocity, while the parameter b reflects the magnitude of the drop in μ associated with the evolution to a new steady state value. *Equation 1* is derived from the

empirical rate and state dependent friction (RSF) laws, developed by Dieterich (1978; 1979) and Ruina (1983), given:

$$\mu = \mu_0 + a\, ln\left(\frac{V}{V_0}\right) + b\, \ln\left(\frac{V_0\theta}{D_c}\right) \qquad (2)$$

where the subscript '0' denotes a reference state, θ is a variable representing the state of the sliding interface and D_c is the (critical) sliding distance over which the evolution effect to a new steady state takes place, after altering the sliding velocity. Although RSF equations are widely used to quantify frictional behavior, they are purely empirical and lack a quantitative mechanistic basis. Such a basis may contribute to out understanding of seismogenesis.

Recently, den Hartog and Spiers (2012) conducted ring-shear experiments on illite-rich gouge, which is similar to natural megathrust fault gouge, at *in-situ* conditions corresponding to ~10km depth along a subduction megathrust (i.e. effective stress (σ_{eff}) = 170 MPa, fluid pressure (P_f) = 100 MPa and Temperature (T) in the range of 150-500°C). These experiments showed a transition from stable to unstable behavior at ~250°C, reverting back to stable sliding at ~450°C, which roughly agrees with the up- and downdip limits of the seismogenic zone. As yet unpublished experiments on muscovite gouge show similar behavior (den Hartog, personal communication, 2012). A mechanism explaining the observed behavior however remains to be determined and emphasizes the urgent need for friction studies on phyllosilicate bearing fault rock materials.

Phyllosilicates are generally believed to be characterized by velocity strengthening behavior, (e.g. Logan and Rauenzahn, 1987; Scruggs and Tullis, 1998) although more recent studies observed sporadic events of stick-slip around a mean value of friction in illite and muscovite aggregates at T ~400-500°C, suggesting they could potentially be velocity weakening under certain conditions (Mariani et al., 2006; van Diggelen et al., 2010; Tembe et al., 2010).

In addition to the controls on sliding stability that is attributed to phyllosilicates with respect to subduction zone seismogenetic behavior, it has been widely proposed that the presence of phyllosilicates may explain the inferred weakness of continental faults (e.g. Shea and Kronenberg, 1992; Wintsch et al., 1995; Wibberley, 1999; Collettini et al., 2009). There is now a general consensus that the bulk strength of a phyllosilicate bearing rock directly depends on the amount and contiguity of the phyllosilicate component (Logan and Rauenzahn, 1987; Shea and Kronenberg, 1992; 1993; Bos and Spiers, 2001; Niemeijer and Spiers, 2005; 2006, Collettini, 2009). It has been shown that phyllosilicate rich rocks can be as weak as the frictional strength of the phyllosilicate at high crustal levels (Shae and Kronenberg, 1992), or as weak as the crystal-plastic flow strength of the phyllosilicate basal plane, at mid- to deep crustal levels (Wintsch et al., 1995). Thus, understanding frictional or shear rheology of phyllosilicates, such as muscovite and illite, is not only relevant to subduction zones, but also to crustal faults, such as the San Andreas fault zone (Lachenbruch and Sass, 1980; Zoback et al., 1987).

Modelling studies on weakening effects phyllosilicates exert on crustal strength, generally assume friction data based on studies as described above (e.g. Bos and Spiers, 2002; Niemeijer

and Spiers, 2005; 2007). However, it is often found that conventional friction experiments are of limited use, because these typically measure the frictional strength of muscovite gouge, whereas for a mechanistic understanding of grain scale slip the local grain to grain friction coefficient is required.

In this study, we conducted direct shear experiments on muscovite single crystals, aimed to gain insight into the grain-scale processes controlling the sliding behavior of muscovite. Our results show an increase in shear strength with pressure and displacement rate and a slight tendency to weaken with temperature. The friction coefficient for muscovite single crystals is reported to be significantly lower than assumed in previous studies which may have considerable implications for crustal strength and subduction zone fault studies and hence for seismogenesis.

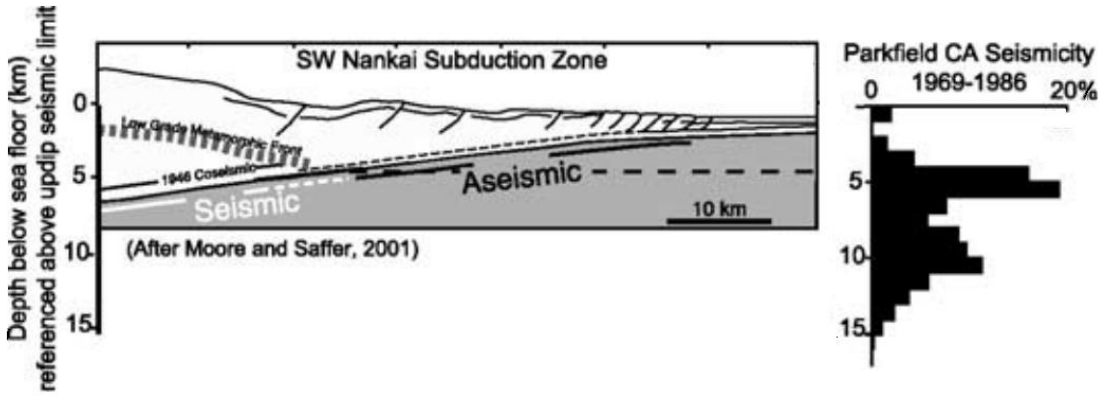

Figure 1: Schematic cross section of the SW Nankai subduction zone, showing the upper transition from unstable to stable sliding behavior. Note the correlation of the upper seismic limit of a subduction zone megathrust (Nankai) with data from a continental strike-slip fault (Parkfield). After Moore and Saffer (2007).

2) Sample material: Muscovite

2.1) Why Muscovite?

Muscovite was chosen as the starting material for the following reasons:

1) It is one of the most common minerals in pelitic metamorphic terrains and is therefore, directly relevant for continental fault and subduction zone megathrust frictional properties.
2) Muscovite is stable over a wide range of temperatures: it is known to form from illite at T > 200° - 295°C (Aja, 1997) and its melting point is 700°- 1250°C, where the lowest values are only reached in the presence of quartz and water, at *in situ* conditions, i.e. confining pressure P_c = 500 MPa (Huang and Wyllie, 1973; van Diggelen et al., 2010).
3) Dehydroxylation of muscovite is known to be fully inhibited up to 500°C (Guggenheim, 1987; Mariani, 2006) and occurs heterogeneously as the strength of the Al-OH bond is strongly affected by the coordination number of the surrounding polyhedra. Therefore, as some OH is lost, the remaining OH is more tightly bound, inhibiting further dehydroxylation (Guggenheim, 1987).
4) The distorted layer structure of muscovite, induced by only two out of three octahedral sites being filled, has been proven to exert anisotropic strength on the (001) basal plane (e.g. Mares and Kronenberg, 1993; see next section). With that muscovite distinguishes itself from other sheet silicates and it allows for additional analysis of the effect of orientation on shear strength.

2.2) Crystal structure of muscovite

Muscovite ($KAl_2(Si_3Al)O_{10}(OH)_2$) is a monoclinic dioctahedral sheet silicate (Putnis, 1992). Charge neutrality is attained by having only two out of three octahedral sites occupied by Al^{3+}, leaving one of every three sites vacant (Güven and Burnham, 1967). This distinguishes muscovite from biotite, which is trioctahedral, with all three octahedral sites taken up by Mg^{2+} and Fe^{2+} (Franzini and Schiaffino, 1963). The regular arrangement of occupied and vacant octahedral sites in muscovite results in distortions of the tetrahedral silicate layers, as well as variations of the K-O bond lengths (Radoslovich, 1960; Apello, 1979; see figure 2). Slip is believed to occur within the weakly bonded interlayer regions (Baños et al., 1983).

The work that must be done to move a dislocation by glide, called the Peierls stress, is determined by the position of the surrounding atoms and is lowest midway between planes of high atomic density (Peierls, 1940). Therefore, dislocation mobility and overall mechanical strength in muscovite may be influenced by variations in K-O bonding, as well as nearby elastic distortions of octahedral layers (Silk and Barnes 1961; Meike, 1989; Mares and Kronenburg 1993). The dioctahedral layer has a wider interplanar spacing in the [110] orientation than in the

[100] or [-110] orientations (Meike, 1989), so that dislocation movement is easiest in the [110] direction. It should be noted however that, as a stacked layer of muscovite is translated and rotated 30° with respect to its parallel counterpart, a [110] orientation is equivalent to [100] in the adjacent layer in a $2M_1$ polytype (Güven and Burnham, 1967; Meike, 1989; Putnis, 1992; figure 2).

The magnitude and direction of the displacement of a dislocation is defined by the Burgers vector. The orientation of the dislocation line with respect to the Burgers vector defines the screw or edge character of the dislocation, i.e. in a screw dislocation, the Burgers vector and the dislocation line are parallel, whereas they are perpendicular to each other in an edge dislocation (Putnis, 1992). Because in muscovite dislocations are affected by the dioctahedral configuration, they are predisposed toward [110] and thus as well to [100], given the rotational offset of stacked layers (figure 2; Meike, 1989). The Burgers vectors reported for muscovite [110] and [100] (e.g. Hirano et al., 1991; Mares and Kronenberg, 1993) are identical to the orientation of the dislocation lines, which suggests muscovite favors screw dislocations.

It is interesting to note that dislocations in the undistorted trioctahedral biotite can be of both screw and edge character, but because the latter type of dislocation is often empirically observed to achieve higher velocities (up to 50 times faster than screw dislocations), the edge dislocations are believed to predominantly facilitate biotite deformation (Meike, 1989).

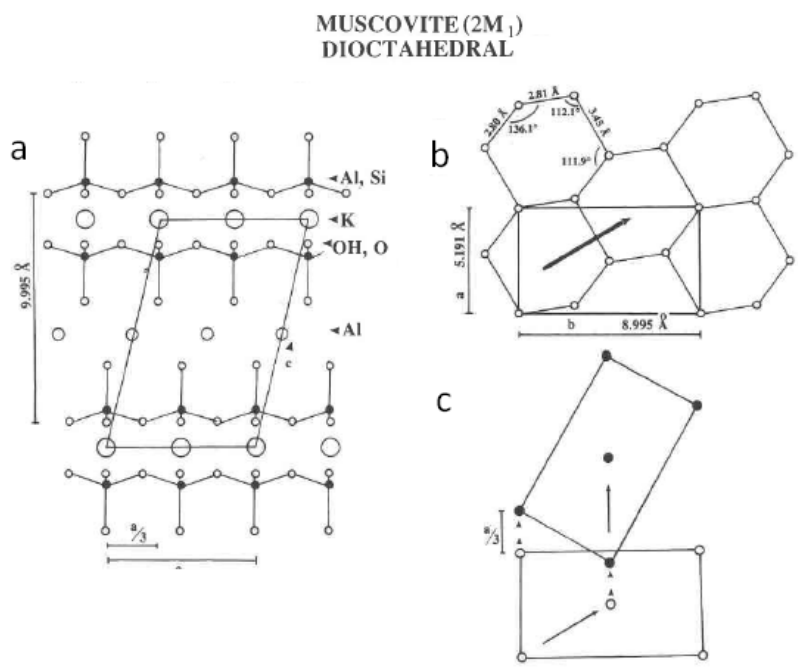

Figure 2: a) diagram of muscovite viewed parallel to the b axis. The fundamental unit cell (as outlined) can be stacked in a variety of polytypes. b) muscovite as viewed normal to (001), represented here as a diagram of the apical oxygen of a tetrahedral layer in the octahedral sheet. The relative distortion of the dioctahedral sheet is due to the vacancy in one of every three octahedral sites, giving the orientation as well as mobility of dislocation preference parallel to [110]. c) The effect of polytypic stacking on dislocation orientation. Alternate layers of the $2M_1$ polytype are translated and rotated 30°. Consequently, [110] of one layer is equivalent to [100] of the adjacent layer. Figure after Meike, 1989.

3) Methods

3.1) Sample preparation

Single crystals of muscovite were purchased from SPI Supplies, USA and received as square plates with dimensions of 25 by 25 mm and a thickness of 0.260 mm (+/- 1 μm). They are clear, with a slight yellowish hue, with faces parallel to the (001) cleavage plane, (i.e. the c – axis is perpendicular to the surface of the plates). The orientations of the crystallographic a and b axes were determined from interference figures using a petrographic microscope. Muscovite plates were cut with a stationary guillotine style metal cutter to 8 by 8 mm squares with sides parallel to the [100] and [010] directions. Abundant cleavage-parallel cracks were present in the samples after cutting. Muscovite samples were not dried before experiments.

In each experiment, two muscovite crystals were stacked parallel to the (001) plane in a crystallographically coherent orientation and loaded with a normal stress applied perpendicular to the (001) plane. Samples were loaded either in an orientation favoring easy crystal plasticity (shear parallel to the [100] direction), or in an orientation unfavorable for plastic behavior (shear parallel to the [010] direction). This was done to evaluate the effect of crystal orientation on muscovite deformation style and shear strength (frictional- versus dislocation glide slip). To inhibit frictional slip at the piston-sample interface, the sample surfaces in contact with the piston were roughened with grinding paper (#80; average particle diameter of 180 μm). Atomic bonding at the interface of the two muscovite crystals was inhibited by roughening the contacting muscovite surfaces with very fine grinding paper (P1200: average particle diameter of 15.3 μm). We do not anticipate the frictional properties of muscovite to be significantly affected by this.

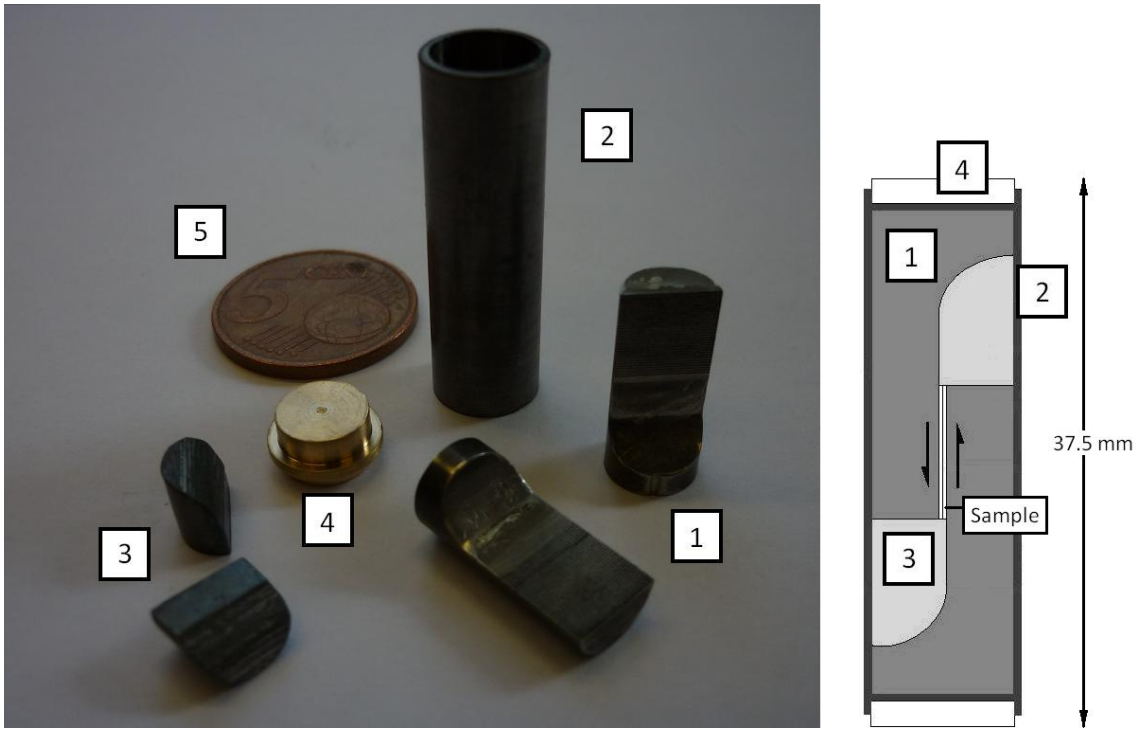

Figure 3: Sample assembly as used in this study. 1, thoriated tungsten '69' direct-shear assembly, in which muscovite samples were loaded; 2, (lead) jacket tube to prevent argon gas from infiltrating the sample pore space; 3, (lead) fillers, installed for piston stability; 4, one of the two brass end-tips to seal off the jacket tube; 5, coin for scale.

The samples were loaded in a direct shear set-up (figure 3), consisting of thoriated tungsten pistons [1] arranged in a 69 configuration (figure 3b), with teeth for grip on the piston-sample interface (30 μm deep, with an interspacing of 0.25 mm). The piston assembly is loaded in a soft metal jacket tube [2] after soft metal fillers [3] are installed to fill up the open space left in the assembly. Subsequently the jacket tube is either sealed by soldering brass tips [4] at both ends (for low temperatures), or by welding (for higher temperatures).

3.2) Experimental Apparatus

Direct shear experiments were performed using a triaxial testing machine[1] (figure 4). This apparatus consists of a water cooled, 1GPa pressure vessel, in which argon gas is used to generate a confining pressure (i.e. the normal stress on the muscovite crystals). Temperatures up to 1200°C are attained with a three-zone Kanthal-AF wire furnace. Temperature is controlled using a proportional-integral-differential (PID) controller and an S-type (Pt/10% Rh) primary thermocouple. The sample temperature is monitored using two S-type sample thermocouples located next to the capsule wall (figure 4b). Calibration runs performed by McDonnell (1997) showed that the temperature gradient over the sample is < 2°C.

[1] See for a more detailed description of this machine McDonnell (1997).

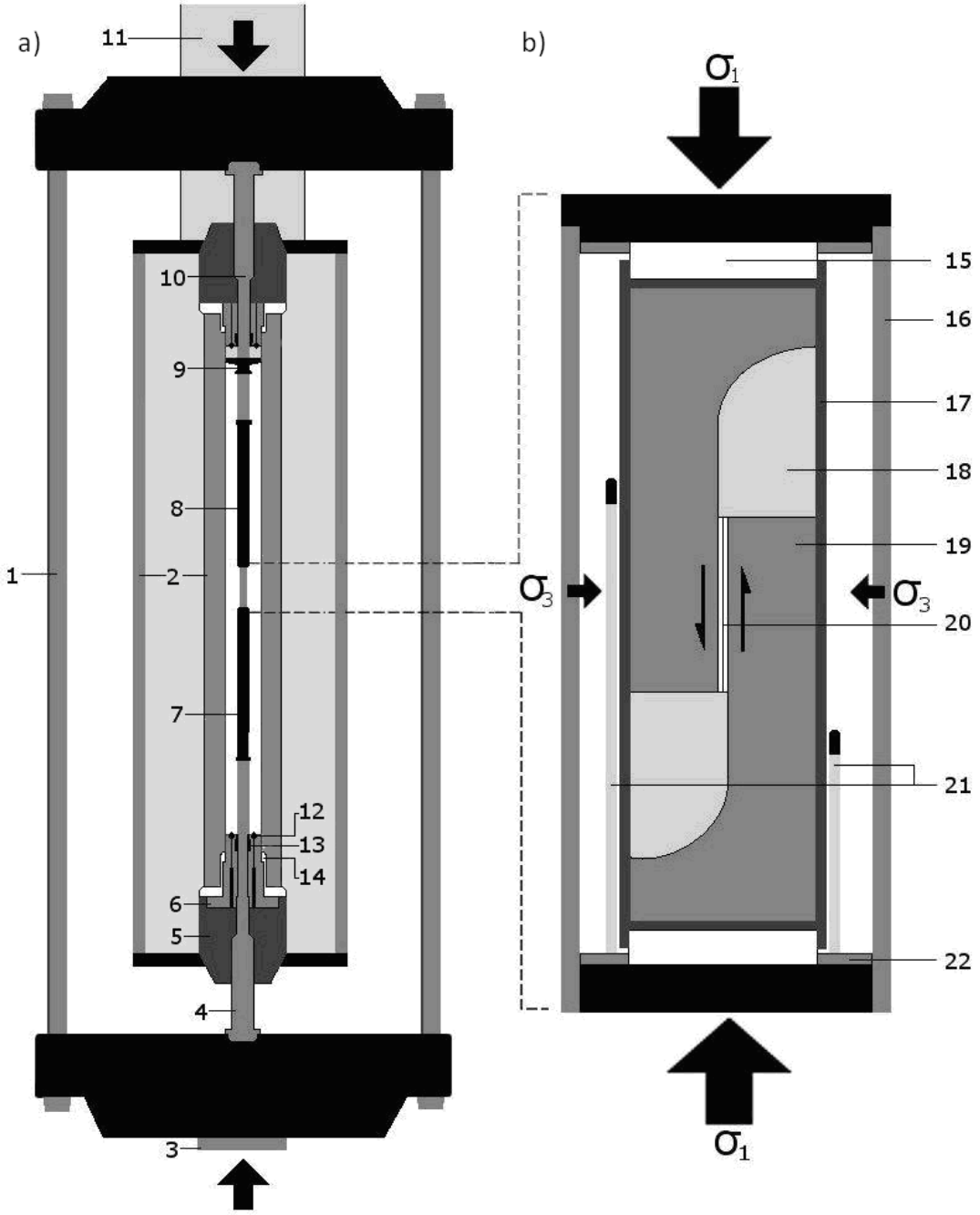

Figure 4: Gas medium, triaxial testing machine used in the present study. a) semi-schematic cross-section of the loading frame and pressure vessel; b) semi-schematic cross-section of the sample assembly. 1, External yoke; 2, water cooled compound vessel; 3, Instron loading ram; 4, steel deformation piston; 5, closure nut; 6, sealing head or end plug; 7, Al_2O_3 section of deformation piston; 8, stationary Al_2O_3 reaction piston; 9, internal load cell; 10, steel compensation piston; 11, load-bearing bridge piece; 12, insulated cone seal for electric lead-troughs; 13, dynamic (Paterson type) seal; 14, external seal; 15, Al_2O_3 anvil; 16, stainless steel pipe; 17, jacket capsule; 18, filler; 19, thoriated tungsten direct-shear piston; 20, muscovite sample; 21, sample thermocouples; 22, stainless steel centering ring.

Axial force is applied to a dynamically sealed deformation piston in contact with the sample, using a horizontally positioned servo-controlled Instron-1362 loading frame. The axial force results in a shear force on the muscovite crystals, and is measured both externally with the 100 kN Instron load cell (accurate to 0.1% of the full-scale output or 0.5% of the indicated load, whichever is greater) and internally with a 100 kN Heard type force gouge (100 kN full scale, ~20N resolution). Constant volume of the pressure vessel during deformation is ensured via a compensation piston coupled to an external yoke. Axial displacement is measured externally using the Instron ram linear variable differential transformer (LVDT, 2 μm resolution). Confining pressure is measured using a strain gauge-type pressure transducer (resolution 0.1 MPa).

3.3) Experimental Procedure

Direct shear experiments have been carried out at temperatures of 150°, 500° and 600°C, displacement velocities of 0.1- 10 μm/s and confining pressures of 270 – 170 MPa. At 150°C, the jacket and fillers were made of lead, whereas at 600°C they were made of silver. At 500°C, we used a silver jacket and aluminium alloy 6082 fillers. During each experiment, the jacketed sample was inserted into the pressure vessel, which was subsequently flushed and pressurized to 300 MPa with argon gas at room temperature. This ensured closure of cleavage parallel cracks induced by sample preparation (see section 3.1). The internal load cell was allowed to re-equilibrate overnight. Shortly before initiation of the experiment, pressure and temperature were adjusted to experimental conditions and the experiment was started when pressure and temperature were found to have stabilized.

During each experiment, the sample was shortened at constant displacement rate, by advancing the deformation piston in position control mode. Each experiment consisted of two phases:

1) Pressure stepping, at constant piston displacement rate (i.e. 1 μm/s; shear strain rate of ~1.92e-3 s^{-1}). For individual steps, the pressure was kept constant at a value being either 270, 220, or 170 MPa, where pressure was decreased in a consistent sequence in each experiment. At the end of each step the piston was moved 0.5 mm away from the sample, thereby fully unloading the sample. The pressure was changed and the loading was restarted after pressure and temperature restabilized.

2) Velocity stepping, at a constant pressure. During the last pressure step at 170 MPa, the displacement rate was instantaneously in- or decreased by one order of magnitude, attaining sliding velocities of 0.1 – 10 μm/s, or shear strain rates from ~1.92e-4 s^{-1} to 1.92e-2 s^{-1}.

In all the experiments, a total shear displacement of ~3 mm was attained. All tests were ended by halting the piston and completely unloading the sample. The final (unloaded) load cell output signal was then compared to the initial (base) output signal, while still at experimental pressure and temperature and the furnace was switched off. The argon was then slowly released from the vessel, reducing the confining pressure. The seals were allowed to relax overnight before the vessel was opened and the sample removed.

3.4) Microstructural analysis

After testing, the jacket was opened up and the sample was carefully removed from the piston. The obtained deformed sample was subsequently vacuum impregnated with commercial Araldite 2020 resin. The resin was cured at room temperature for 48 hours. The cured samples were cut perpendicular to the shear plane and parallel to the shear direction and polished, for analysis using a Leica DMRX microscope.

3.5) Data Processing

In a triaxial machine as described above, the internal load base signal at zero applied load is dependent on pressure and is routinely measured prior to, and after every deformation run and checked for consistency. Shear stress on the sample was calculated from the internal axial force, corrected for apparatus stiffness, pressure variations and jacket strength, assuming constant volume, no effective area change, and homogeneous deformation.

3.5.1) Jacket Corrections

Appropriate jacket corrections were generally determined using data compiled by Frost and Ashby (1982). These authors determined rate dependence and specific material strength of a number of metals and alloys, for a range of temperatures, assuming no pressure dependence. At all times during the experiment, $T \geq 0.4T_m$ of the jacket material, so that Dorn-type flow is assumed. For a more elaborate description of jacket corrections, the reader is referred to the Appendix.

Even though jacket materials were selected that yielded minimal strain hardening, an artificial hardening effect on sample mechanics could not be fully excluded. Because of that, in pressure stepping tests, the response of sample shear strength on decreasing confining pressure is easily masked by ongoing displacement hardening of the metal jackets. To account for this effect, the hardening slope at each pressure step was extrapolated linearly up to the amount of total displacement where muscovite at the next pressure yielded (see figure 5). The equivalent of the difference in strength between the extrapolated point and the yield point of the sample at the next pressure step was subsequently subtracted from the initial yield point at 270 MPa. That way, the effect of jacket strain hardening is fully excluded in analysis on pressure dependence. It is noted that with this procedure a potential intrinsic hardening effect of muscovite is neglected.

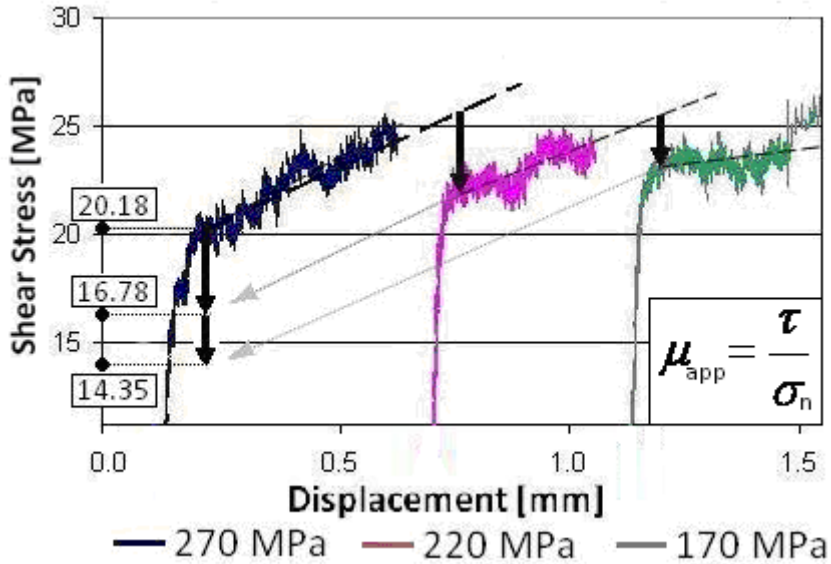

Figure 5: Detail of figure 7, sample M3, illustrating the procedure by which friction coefficients were obtained. To evaluate pressure dependence whilst steady state flow has not yet been reached, the contribution to strength due to displacement hardening is subtracted from the initial yield point at 270 MPa. Hence, shear stresses denoted here represent the expected yield points of muscovite single crystals at 270, 220 and 170 MPa, neglecting displacement hardening of both jacket material and potentially of sample material. As is thus visualized, pressure stepping has a small, but clear influence on the strength of muscovite; shear strength at yield for P_c = 270, 220, and 170 MPa, is inferred being 20.18, 16.78 and 14.35 MPa, respectively.

3.5.2) Corrections for effective area

It has been shown by Verberne et al. (ongoing research, personal communication, 2012) that with ongoing shear, a continuously decreasing effective area on which normal stress is applied, results in decreasing shear strength, i.e. an apparent weakening effect that is non-intrinsic to sample properties. In a direct shear set-up, as used by Verberne et al. and this study, it can be argued that apparent strengthening or weakening due to in- or decreasing effective area is controlled by the relative strength of the filler material; i.e. with ongoing shear, filler material is progressively wedged underneath the sample material which can either result in strengthening of the sample by adding to the effective area, or it can be of no load bearing support, resulting in weakening of the sample. Whichever of these is applicable seems to depend on the relative strength of the filler materials.

Adding to the ambiguity, Verberne et al. noted that determining an appropriate correction for changing effective area was variable for each individual experiment, so that its application is in this study dismissed.

3.5.3) *True and apparent friction coefficients*

When discussing frictional behavior in materials, authors generally distinguish amongst *apparent* friction coefficient and what we from here on will call the *true* friction coefficient. The latter parameter is usually described in Mohr-Coulomb analysis where *true* μ defines the slope

of the shear strength of a material versus normal stress, where it intersects the normal stress axis at a point defining the cohesive shear strength of a material (S_0). Consequently, in experimental studies the true friction coefficient is obtained by imposing varying normal stresses on the sample (in this study by means of confining pressure stepping). The *apparent* friction coefficient is simply the ratio of shear stress over normal stress, at a fixed confining pressure and assumes no cohesive shear strength. The two parameters usually do not differ significantly in magnitude, but as they are generatively different, it is indispensible that they are considered separately.

4) Results

4.1) Mechanical behavior

Shear stress versus displacement curves for the present experiments are shown in figure 7. Recall that each experiment consisted of 1) a pressure stepping phase, where pressure was reduced from 270, to 220, to 170 MPa in consecutive order, and 2) a velocity stepping phase, where velocity was instantaneously in- or decreased one order of magnitude relative to the base velocity 1 μm/s, during shearing. The graphs shown here are for experiments performed at 150° and 500°C, where the orientation of the muscovite crystals with respect to the shear direction was controlled to either inhibit or enhance dislocation glide, i.e. parallel to the [010] and [100] directions, respectively (Meike, 1989; Hirano et al., 1991; Mares and Kronenberg, 1993). The experiment performed at 600°C is not shown, as the strength of the silver jacket/filler set-up was about equal to that of the sample and we could therefore not adequately correct for it. In each graph, the magnitude of the jacket correction under the relevant conditions is given for 1 μm/s.

Figure 6: Example of the sample assembly loaded in a lead jacket with brass end-tips, before and after deformation. Note how the filler material bulges out after deformation.

4.1.1) Effect of temperature and pressure

It should be noted that sample M1 was not fully unloaded before depressurizing from 270 to 220 MPa, which resulted in the initial base signal at 220 MPa not being zero. The unloaded base signal however was checked for being zero at the end of the 220 MPa pressure step so that the result depicted here can be viewed with confidence.

All experiments show a rapid increase in shear stress followed by an apparent yield point and by subsequent displacement hardening. The sample strength at all conditions tested is slightly

pressure sensitive where shear strength decreases with decreasing confining pressure, yielding an apparent friction coefficient (ratio of shear stress over normal stress, at a fixed confining pressure) ranging between 0.074-0.094 (figure 9). Shear stress versus normal stress plots are presented in figure 10, yielding true friction coefficients of 0.051, 0.053 and 0.058 for M1, M2 and M3 respectively and 0.116 for M4. Shear strength, at least when comparing M3 to M1, seems to be somewhat lower at elevated temperatures, but otherwise temperature does not seem to have a great effect. In general, the mechanics of samples M1, M2 and M3 are comparable, whereas M4, sheared at 500°C parallel to the [010] direction, exhibits a higher initial yield point, a pressure dependence that is more pronounced and an apparent friction coefficient that increases with decreasing confining pressure.

4.1.2) Effect of sliding velocity

At 150°C, muscovite yields velocity strengthening behavior when orientated to enhance dislocation glide [100], and velocity neutral to slightly velocity strengthening behavior when orientated to inhibit dislocation glide [010]. Both samples sheared at 500°C exhibit velocity strengthening behavior that is slightly more pronounced than for samples sheared at 150°C. At 150°C, velocity up- and down stepping results in a direct in- or decrease of strength, respectively, followed by a progressive evolution to steady state sliding. At 500°C this evolution effect is virtually absent, so that the direct effect on strength of velocity stepping alone constitutes the rate dependence of muscovite at these conditions.

4.1.3) Strength fluctuations

After yield, small periodical strength in- and decreases are exhibited, which are most pronounced at low T and high P_c. These strength fluctuations seem systematic and are characterized by a wavelength of about 0.25 mm. With increasing total displacement the amplitude of this wavy pattern decreases, until it becomes undistinguishable at approximately 2 mm total displacement.

a) **Enhancing Plastic Flow**

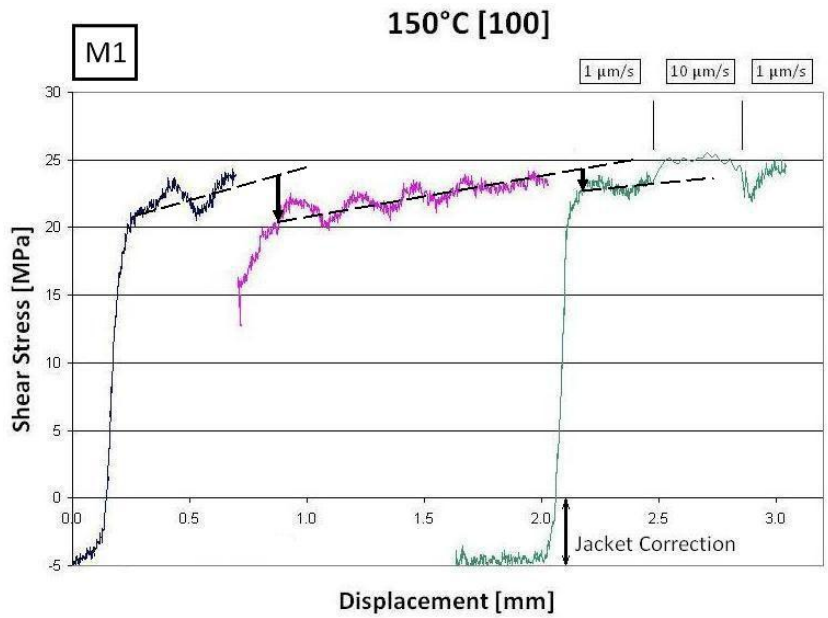

b) **Inhibiting Plastic Flow**

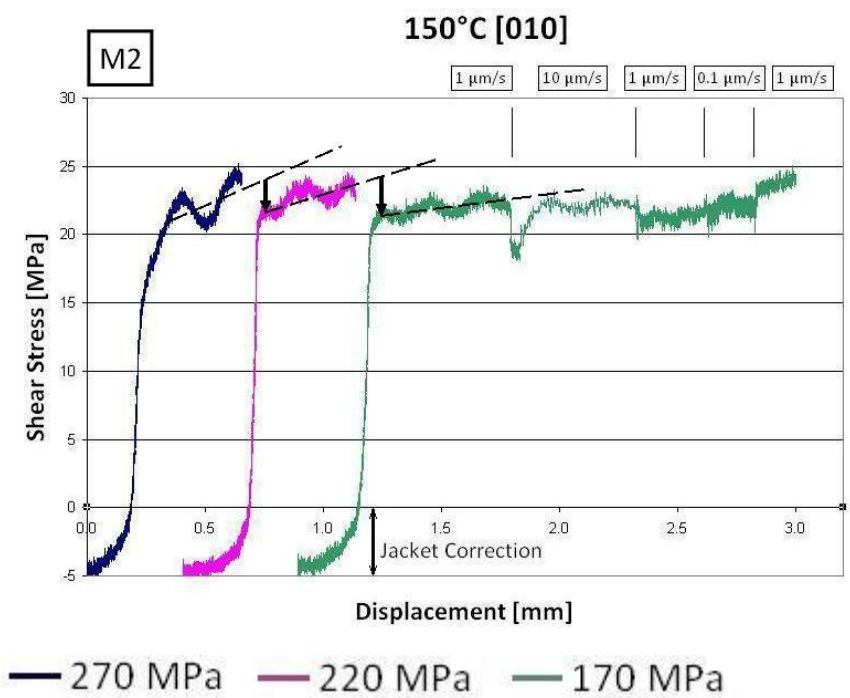

Figure 7: Plots showing Shear Stress versus Displacement of pressure/velocity stepping experiments. First, pressure was reduced from 270, to 220, to 170 MPa in consecutive order and second, at 170 MPa, velocity was instantaneously increased or decreased by one order of magnitude relative to the base velocity 1 μm/s, during shearing. Note that figures a and c represent samples M1 and M3, sheared in a direction that enhances plastic flow, whereas figures b and d shows plots for samples M2 and M4, sheared in a direction inhibiting plastic flow. Samples show pressure sensitivity, most clearly exhibited by sample M4. At all conditions samples yield velocity strengthening behavior, where sample M2 tends to velocity neutrality. The magnitude of the appropriate jacket correction is given in each graph.

c) Enhancing Plastic Flow

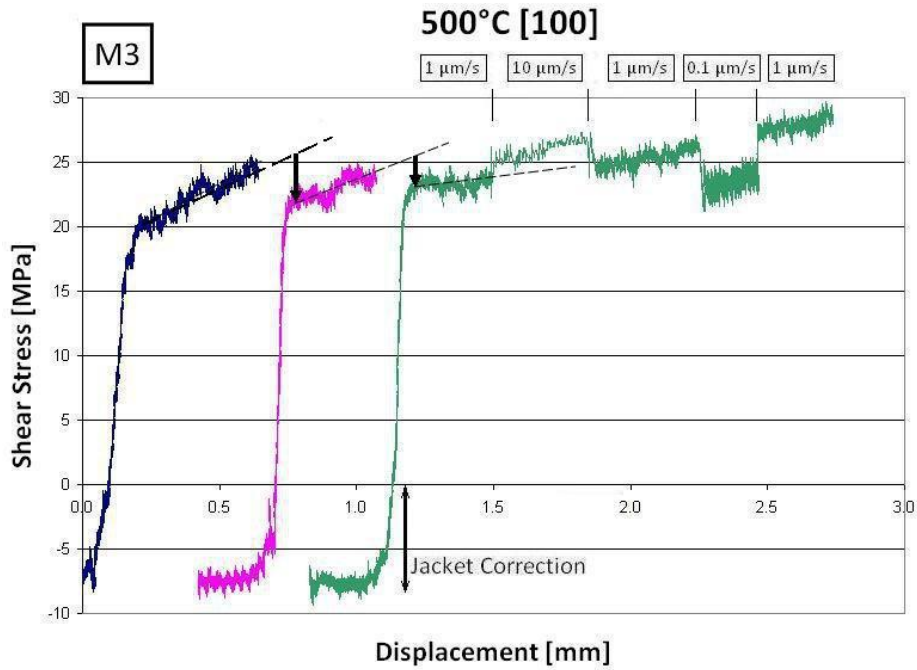

d) Inhibiting Plastic Flow

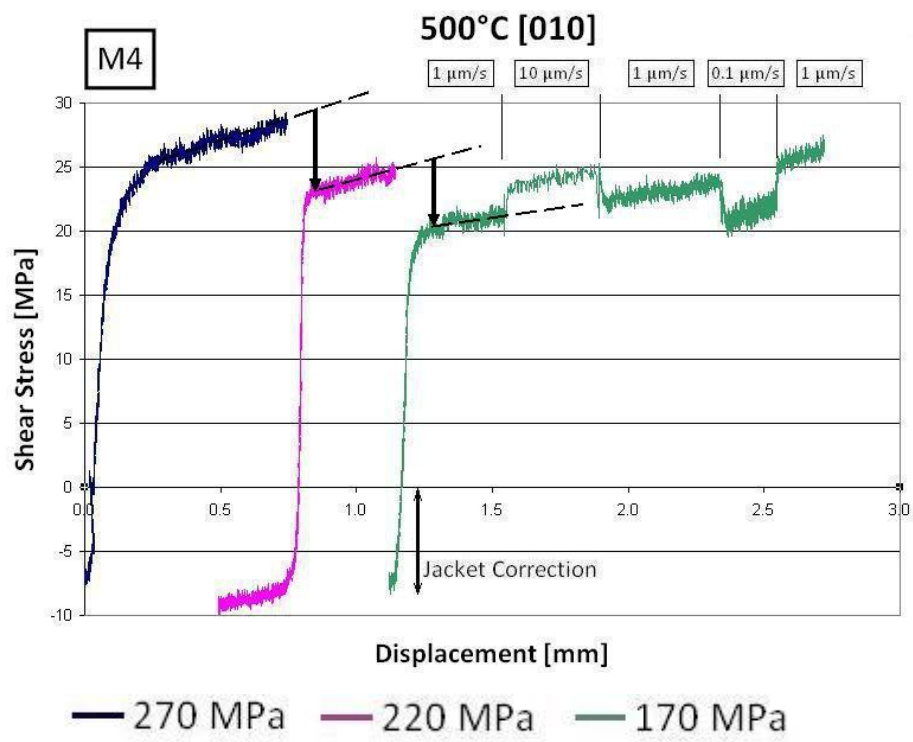

Figure 7: Continued.

4.2) Microstructures

At all conditions tested, the samples remained intact as two separate single crystals. The microstructure developed in each experiment was investigated and figure 8 shows an overview of the resulting micrographs. Microstructural features are discussed for each temperature separately, considering characteristics found throughout the sample only.

4.2.1) 150°C

Sample M1, sheared at 150°C, parallel to the [100] direction, favoring plastic flow, generally retains its straight foliation trace (fig 8a). Sporadically, narrow kink zones have developed, displacing the foliation trace consistent with shear direction (fig 8b). The foliation trace of sample M2, sheared parallel to the [010] direction, inhibiting plastic flow, is slightly more wavy than M1 (fig 8c; d). Unlike M1, M2 lacks kink bands, but cleavage parallel cracks are slightly more abundant in M2 than in M1 and in both samples run all along the sample length.

4.2.2) 500°C

Deformation in sample M3, sheared at 500°C in the [100] direction, is localized in narrow kink bands with axial traces at 30° to 60° to the foliation trace and recurring with an interspacing in the order of 60-100 μm (fig 8e). These shear bands offset the foliation by 2-5 μm, in a sense consistent with the shear direction (fig 8f). In some locations deformation within these kink bands was sufficiently intense to allow for the formation of a secondary cleavage, 30° to the original foliation. Cleavage opening in some locations clearly offsets this secondary cleavage and seems to have occurred after their formation (fig 8e; small arrows). Brittle processes other then cleavage opening are not clearly evidenced. Unlike M3, the foliation trace in M4, sheared parallel to the [010] direction, is relatively undistorted (fig 8g). Sporadically, weakly developed, high-angle kink bands are present, slightly bending the mica layers in a direction consistent with shear direction (fig 8h). Unlike the other samples the cleavage has remained fairly coherent (i.e. cleavage opening is less intense compared to other samples) and brittle processes are absent, apart from several small, localized cracks cutting across the cleavage trace (fig 8g; h; small arrows).

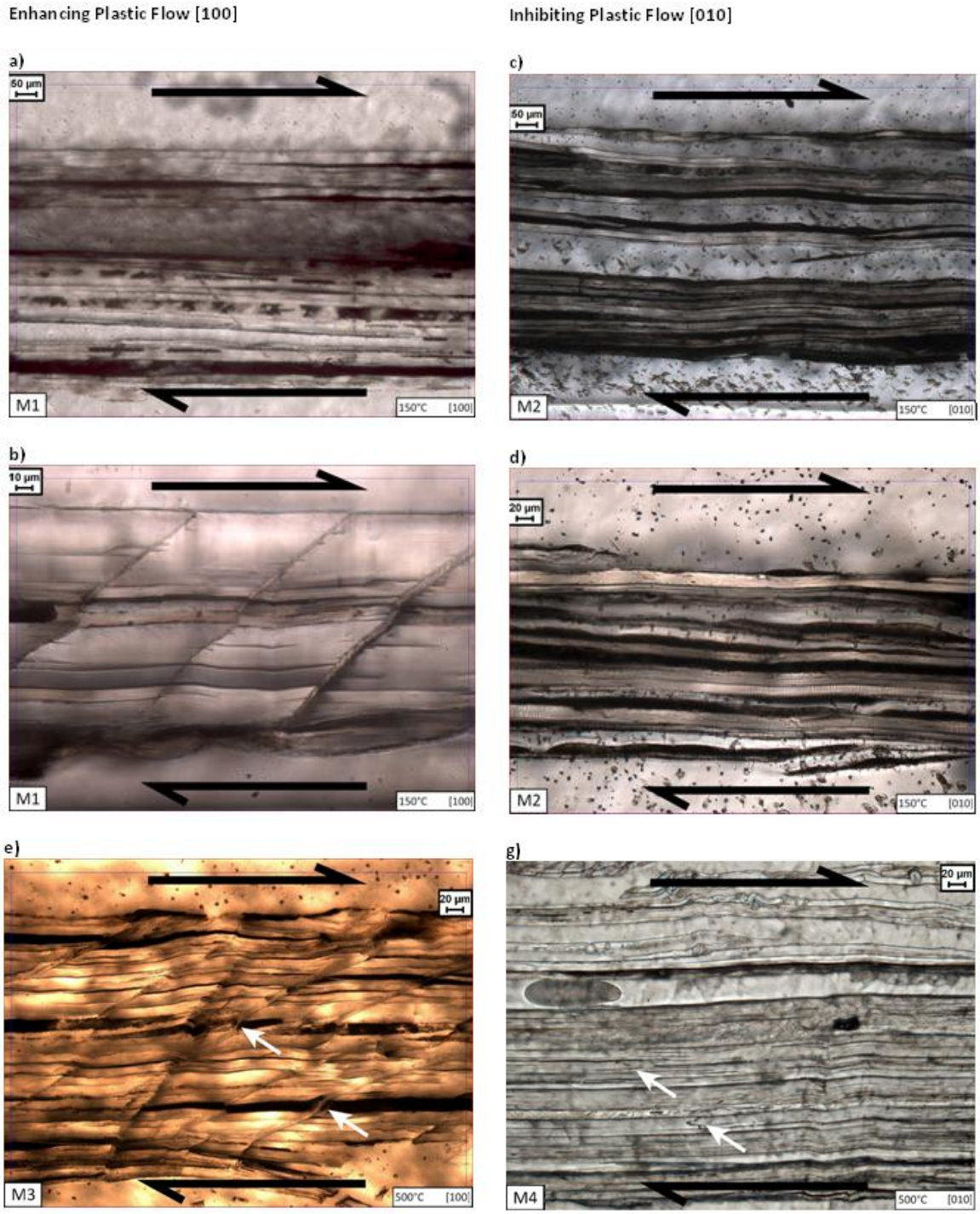

Figure 8: Microstructures of samples M1 through M5 after deformation, viewed through a Leica DMRX microscope. a); b), sample M1, sheared at 150°C, in a direction enhancing plastic flow; c); d), sample M2, sheared at 150°C, in a direction inhibiting plastic flow; e); f), sample M3, sheared at 500°C in a direction enhancing plastic flow. White arrows indicate secondary cleavage being offset by cleavage opening; g);h) sample M4, sheared at 500°C in a direction inhibiting plastic flow. White arrows indicate small cracks, cutting across the cleavage trace; i); j), sample M5, sheared at 600°C in a direction enhancing plastic flow. Arrows indicate the shear sense.

Enhancing Plastic Flow [100]

Inhibiting Plastic Flow [010]

f)

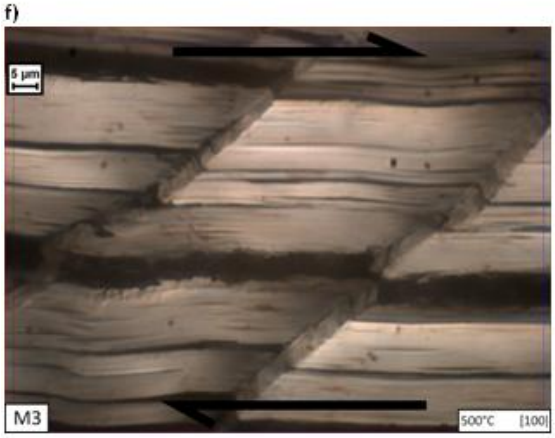

h)

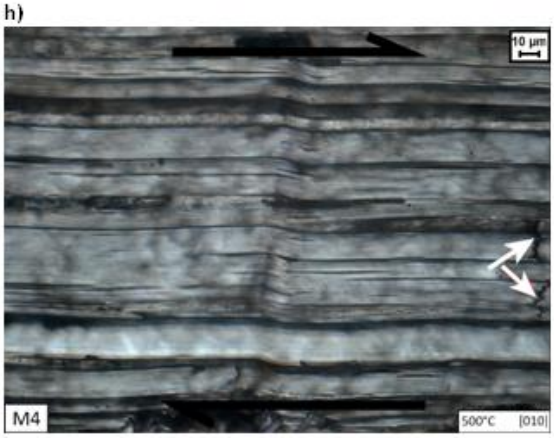

i)

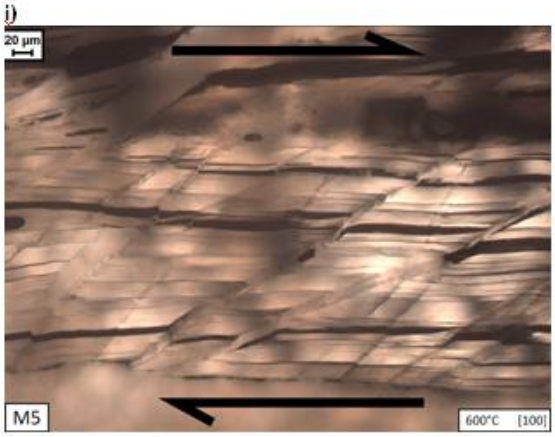

j)

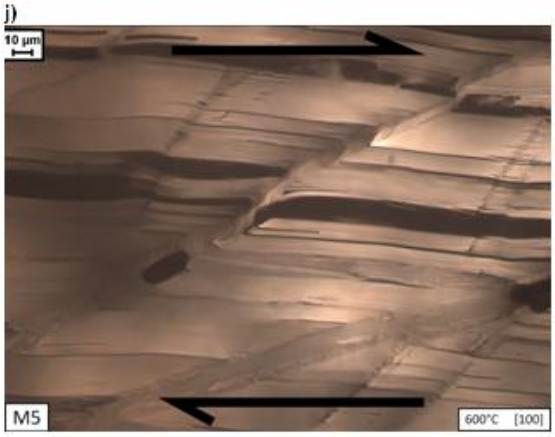

Figure 8: continued

4.2.3) 600°C

Similar to M3, deformation is localized in kink bands in M5, which is sheared parallel to the [100] direction, enhancing plastic flow (fig 8i). Two sets of kink bands are formed, at 30° and 60° to the main foliation trace. The first set is strongly developed and has a wavelength of approx. 50-100 μm and drags the foliation trace along the kink band by about 5-20 μm, in a manner consistent with shear direction (fig 8j). The second set of kink bands is characterized by small scale (localized within 2-5 μm, parallel to the foliation), sharp kinking of the foliation. However, it is less well developed in general and sometimes present as lined up dilatational features only. Additional dilatation is associated with the creation of cleavage opening that in some locations clearly offsets kink bands.

5) Discussion

Pressure stepping experiments consistently yielded decreasing strength with decreasing normal stress, with a *true* coefficient of friction of 0.051 - 0.116 (figure 10) meaning that at least to a certain extent muscovite sliding behavior was normal stress dependent, suggesting at least partial friction control. These values are significantly lower than previously reported for muscovite gouge and immediately draw attention to previous work on muscovite frictional behavior, which will be discussed in section 5.2. We will go on in section 5.3, to consider the difference in rheology between muscovite gouge and single crystals. Finally, section 5.4 assesses the implications of our observations on crustal strength and hence on seismogenesis.

At low T and high P_c, periodical strength fluctuations were observed. These fluctuations are systematic and recur with a wavelength of 0.25 mm. Given the wavelength of these strength fluctuations and the interspacing of the piston teeth (see section 3.1), it is likely these are an effect of the pistons, rather than being an intrinsic property of the sample. It is hypothesized that at elevated confining pressures, the piston teeth at both piston-muscovite interfaces exerted incremental relief on the muscovite-muscovite interface, causing periodical strength in- or decreases with displacement, of which the period is controlled by the interspacing of the piston teeth (0.25 mm). Whether the virtual absence of these mechanical fluctuations in samples M3 and M4 is caused by elevated temperature, or by a different jacketing material remains unclear.

5.1) Frictional versus plastic behavior

Microstructural analysis reveals a clear trend in deformation style: kink bands form easier at elevated temperatures, but their formation is strongly inhibited when muscovite is sheared parallel to [010]. This latter observation draws attention to previous reports on dislocation glide parallel to the basal plane of muscovite, which is noted to be easier in the [100] than in the [010] direction (Meike, 1989; Hirano et al., 1991; Mares and Kronenberg, 1993). This suggests that kink band formation as observed in this study is promoted or even controlled by dislocation glide. At 150°C, kink bands form sporadically and only when sheared parallel to [100]. This suggests that, although dislocation glide parallel to the basal plane cannot be entirely ruled out, frictional processes mostly facilitated deformation at this temperature.

At elevated temperatures kink bands form more readily, although even at 500°C kink band formation is strongly inhibited when shear is parallel to the [010] direction. In the case of sample M5, given the recurrence and average offset of kink bands it is possible deformation was mostly facilitated by crystal plastic processes. Pure plasticity however does not involve dilatational or brittle features, whereas cleavage opening is clearly portrayed in the microstructures of all of the samples. At locations of cleavage opening, foliation cross-cutting kink bands like those extensively formed in sample M3 and sample M5 are offset perpendicular to the foliation trace (fig 8e; small arrows) but definitely not in a manner consistent with shear direction. This makes

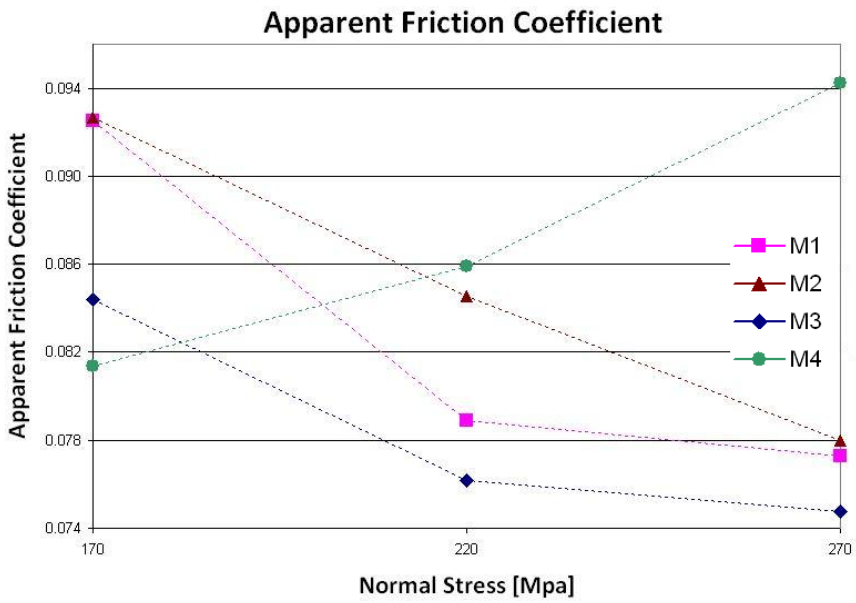

Figure 9: Apparent friction coefficients for the pressure stepping phase of each experiment (v = 1µm/s). Apparent friction coefficients are calculated by dividing the shear stress at yield by the relevant confining pressure (i.e. normal stress) after subtraction of the strength contribution of the jacket and of jacket hardening. M1: 150°C, sheared in a direction enhancing plastic flow; M2: 150°C, sheared in a direction inhibiting plastic flow; M3: 500°C, sheared in a direction enhancing plastic flow; M4: 500°C, sheared in a direction inhibiting plastic flow. Note that the apparent friction coefficient disregards cohesive shear strength and, as values are calculated for a fixed normal stress, also disregards the actual response of a material to changing normal stress. Apparent friction coefficients at 170 MPa are compiled for comparison with previous studies in *table 1*.

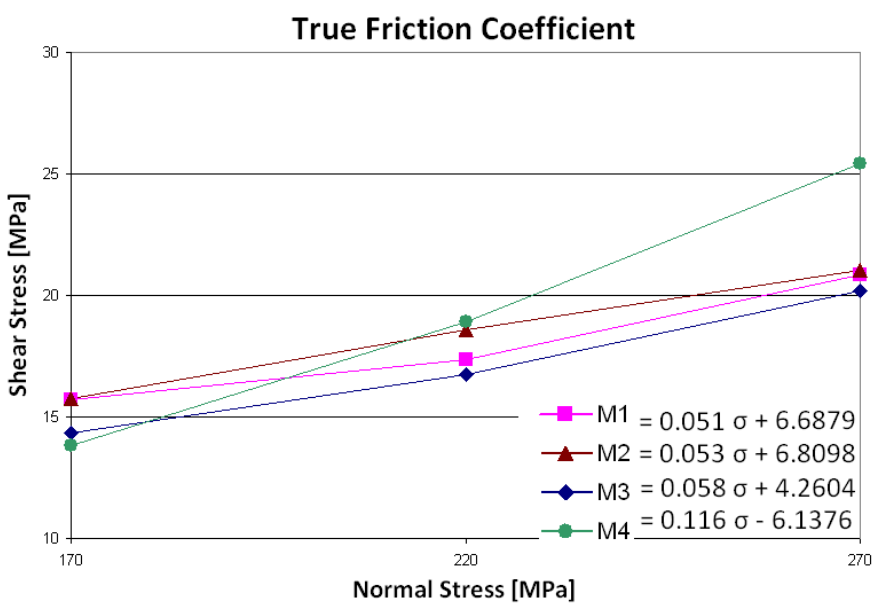

Figure 10: Shear stress versus normal stress plot for the pressure stepping phase of each experiment. The slope defines the true coefficient of friction, whereas the intersection with the normal stress axis at zero MPa defines the cohesive shear strength. For experimental conditions see caption figure 9. Note the pronounced difference in friction coefficient of M4 with respect to the other samples. The slope of sample M4 might however be slightly less steep than suggested here, as negative cohesive shear strength is physically unrealistic.

it likely that samples were deformed through a combination of frictional and crystal plastic processes allowing for interlayer bond rupture, where actual cleavage opening would be an effect of depressurizing the vessel after finalizing the experiment.

From figure 10 it is clear that at 500°C, muscovite sheared in a direction inhibiting plastic flow (i.e. parallel to [010]) is slightly stronger as well as twice as pressure sensitive compared to muscovite sheared in a direction enhancing plastic flow (i.e. parallel to [100]), at the same temperature. This suggests that at 500°C, the direction in which muscovite is sheared, controls the degree to which it behaves in a frictional manner. This is supported by the difference in deformation style that is observed in the microstructure. At 150°C, on the other hand, there seems to be no difference in mechanical response when muscovite is sheared parallel to [100] or to [010]. Whether this lack of mechanical difference at this temperature is an intrinsic characteristic of muscovite single crystals, a procedural flaw in experimental set-up, or perhaps even an indication for the margin of error that should be considered for this type of experiments will only be clear with more data.

Although there is a striking difference between muscovite microstructures, the shear strength hardly seems to be affected by temperature or sliding direction. This implies that either 1) the amount of shear stress required to plastically deform muscovite is virtually equal to that required to deform muscovite in a frictional manner, or 2) the shear strength of muscovite is not controlled by the formation of kink bands.

5.2) Comparison with previous work

5.2.1) Apparent friction coefficient

Previous studies on muscovite gouge at room temperature have yielded a consistent *apparent* friction coefficient of 0.39 ± 0.03 (Scruggs and Tullis, 1998; Morrow et al., 2000; Moore and Lockner, 2004). However, it is not entirely clear to what extent friction coefficients obtained in these studies can be considered as steady state values. As muscovite gouge is known to harden with displacement, the magnitude of the friction coefficient is dependent on the amount of shear strain (e.g. Mariani et al., 2006; van Diggelen et al., 2010). For instance, based on data compiled by van Diggelen et al. (2010), the apparent coefficient of friction of muscovite gouge sheared at T = 400°C, v = 1 μm/s and σ_{eff} = 100 MPa, is 0.25 at yield, but increases to 0.37 at steady state, at a shear strain of 30. Therefore, for a consistent comparison with previous work, this study compares apparent friction coefficients reported by Mares and Kronenberg (1993), Mariani et al. (2006) and van Diggelen et al. (2010), at yield (*table 1*).

Table 1: Comparison of apparent friction coefficients based on Mares and Kronenberg (1993), Mariani et al. (2006), van Diggelen et al. (2010) and this study, distinguishing between muscovite gouge and single crystals. P_{eff}, P_p and v are effective pressure, pore fluid pressure and displacement velocity, respectively. For single crystals, the shear direction with respect to the crystal structure is given, i.e. [100] implies shear parallel to the basal plane and the [100] direction.

Comparison of Apparent Friction Coefficient of Muscovite at yield						
	Mariani et al. (2006)	van Diggelen et al. (2010)	Mares and Kronenberg (1993)		This study	
	GOUGE		SINGLE CRYSTALS			
T [°C]			[100, 110]	[010, 310]	[100]	[010]
100			0.075 - 0.1225	0.135 - 0.145		
150		0.23			0.093	0.093
200			0.04 - 0.075	0.115 - 0.12		
400	0.29	0.25	0.055 ± 0.02	0.08 ± 0.012		
500	0.35	0.33			0.084	0.081
600	0.36	0.32				
Comments	P_{eff} = 172 Mpa	P_{eff} = 100 Mpa	P_{eff} = P_c = 200 Mpa		P_{eff} = P_c = 170 Mpa	
	v = 1.8 μm/s	v = 1 μm/s	v = 0.33 μm/s		v = 1 μm/s	
	P_p = 34 Mpa	P_p = 100 Mpa	no P_p		no P_p	
			Relatively large sample to sample variations			

Table 1 clearly shows that at each temperature the apparent friction coefficient of muscovite gouge is 0.2-0.3 higher than measured for single crystals[2]. Overall, the apparent friction coefficients reported in this study for P_c = 170 MPa compares reasonably well with Mares and Kronenberg (1993), especially in light of the differences in experimental conditions (see *table 1*).

For muscovite single crystals, the apparent friction coefficient is found to be slightly lower at elevated temperatures, whereas an inverse relation with temperature is obtained for muscovite gouge. Mares and Kronenberg (1993) showed a rather large effect of temperature on the sliding strength of muscovite single crystals, as μ is generally 40-50% lower at 400°C than at 100°C. They attribute this temperature dependence to deformation being entirely facilitated by crystal plasticity. In this study, a temperature dependence of μ is shown, but to a lesser extent (μ is ~ 10% lower at 500°C, than at 150°C). Given that dislocation glide exhibits temperature dependence about 5 times higher than yielded by our samples, as shown by Mares and Kronenberg (1993), it follows that dislocation glide played a lesser, or even minor role in deformation of muscovite single crystals in this study. This suggests an important role of frictional processes for deformation in our samples.

A mechanical anisotropy on the basal plane (i.e. shear strength is higher when muscovite is sheared parallel to [010] than to [100], on the basal plane), as reported by Mares and Kronenberg (1993) is not evidenced by the apparent friction coefficient obtained in this study. This however, perhaps points out the shortcomings of mechanical analysis based on apparent friction coefficients as cohesive shear strength is therein disregarded, as well as the actual

[2] Note that in this study, strain hardening is entirely neglected as a consequence of correcting for jacket hardening (section 3.5.1). This assumption is supported by Mares and Kronenberg (1993) who did not observe any significant hardening effects for muscovite single crystals.

response of a material to changing normal stress. The *true* coefficient of friction may be of more relevance here (figure 10).

5.2.2) Pressure sensitivity

The pressure sensitivity of strength of mica schist has been reported to decrease from $\mu \approx 0.5$ at $P_c < 100$ MPa, to $\mu < 0.1$ at $P_c > 200$ MPa (Shea and Kronenberg, 1992). Comparable results have been shown for muscovite single crystals, as a transition was reported from pressure dependent basal shear strength in muscovite single crystals at $P_c < 50$ MPa, (apparent $\mu \approx 0.4$) towards pressure independent strength at $P_c > 100$ MPa (apparent $\mu \approx 0$; Mares and Kronenberg, 1993). Additionally, these authors showed that at confining pressures high enough to inhibit frictional sliding in muscovite ($P_c > 100$ MPa), optical microscopy yielded similar dislocation arrangements developed in samples deformed at 20°C and 400°C. This is substantiated by Meike (1989), who performed in situ TEM analysis and reported moving dislocations even at room temperature.

Confining pressures and hence normal stresses imposed in this study are well over 100 MPa, proposed by Mares and Kronenberg (1993) to be the threshold value to inhibit frictional sliding ($\mu \approx 0$). However, for a detailed look on the mechanical behavior of muscovite single crystals at elevated confining pressures, their work might not provide sufficient data. In their work, strength evaluations are mostly based on samples sheared at only one confining pressure, (P_c = 200 MPa), where the determination of the true friction coefficient is based on only several data points representative for higher confining pressures. The effect of pressure is evaluated regardless of shear direction, despite the shown mechanical anisotropy on the basal plane. In addition, sample to sample strength variations are noted to be relatively large. As the true friction coefficient at these elevated confining pressures is likely to be very low, the quality of data reported by Mares and Kronenberg (1993) might not be sufficient to constrain sliding behavior at these conditions.

5.2.3) Mechanisms for muscovite single crystal deformation

Results from this study suggest that even at elevated P_c, muscovite single crystals are still pressure sensitive. Based on the following points it is here proposed that muscovite single crystals deform through a combination of crystal plastic and frictional processes, where strength is mostly controlled by grain boundary sliding friction:

1) Shear strength of muscovite single crystals is found to be only slightly dependent on temperature. Crystal plastic deformation in muscovite single crystals has previously been shown to exhibit temperature dependence about five times larger than observed in this study, which suggests that frictional, rather than plastic processes were dominant in our samples;

2) Shear strength is slightly pressure sensitive with a true friction coefficient of ~ 0.055 up to 0.12;

3) The frictional strength of muscovite single crystals is rate-dependent under all conditions investigated, which suggests a contribution of crystal plasticity;

4) Kink bands form readily with elevated temperatures but their formation does not seem to affect the shear strength of muscovite;

5) Brittle/frictional processes associated with interlayer bond rupture and cleavage opening are observed in the microstructures at all the conditions tested;

6) At least at 500°C shear strength as well as pressure sensitivity increases when single crystals are sheared in a direction inhibiting dislocation glide;

7) Given the continuity of foliation cross cutting features like kink bands as portrayed in M3 and M5, combined with the fact that at all conditions tested, crystals have remained intact throughout the experiments, it is likely friction mostly occurred on the muscovite-muscovite interface.

5.3) Gouge versus single crystals

Muscovite gouge is, for all conditions tested, systematically stronger than single crystals and is reported to harden with temperature up to 700°C (Mariani et al., 2006; van Diggelen et al., 2010), whereas the strength of muscovite single crystals decreases with temperature. Evidently, there is a pronounced difference in mechanical behavior of muscovite gouge with respect to muscovite single crystals. In this section we will shortly address these differences and discuss possible microphysical explanations for the observed behavior.

5.3.1) *Shear Strength*

The friction coefficient of muscovite gouge is, for all conditions tested, systematically 0.2-0.3 higher than measured for single crystals (see also Collettini et al., 2009). In muscovite gouge, even at steady state sliding, not all muscovite grains are perfectly orientated for easy slip (e.g. Scruggs and Tullis, 1998) It may be argued that this geometrical misfit of grains serves as an obstacle for sliding, which would make it more difficult to deform. Indeed, this may also be the cause of strain hardening, often observed for gouge (Mariani et al., 2006) although it has also been suggested that strain hardening is caused by pervasive cataclasis and associated compaction with ongoing shear, leading to a change in dilatation angle and an increase in friction coefficient (van Diggelen, 2010).

5.3.2) Effect of temperature

Gouge hardens with temperature, whereas single crystals slightly weaken with temperature. An increase of muscovite gouge strength with temperature may be attributed to thermally activated diffusive or plastic flow processes in bands where pronounced grain size reduction has occurred. This would induce compaction and hence hardening of the material (van Diggelen et

al., 2010). In single crystals material transport would play less a role in controlling sample strength, so that increasing temperature would only weaken muscovite through increasing crystal plasticity.

5.3.3) Controls on Rate-dependence

Both gouge and single crystals are observed to be rate-dependent (Mares and Kronenberg, 1993; van Diggelen et al., 2010; den Hartog and Spiers, ongoing research; this study). Rate-dependency in phyllosilicate rich materials is either governed by pressure solution (Bos and Spiers, 2002; Niemeijer and Spiers, 2007) or by crystal plastic processes (Mares and Kronenberg, 1993; Wintsch et al., 1995). Evidently, when a material exhibits rate-dependence, deformation must be facilitated by more than frictional sliding only. Therefore, it might be of interest here to address implications of a threshold normal stress limit (i.e. > 100 MPa) to fully inhibit frictional sliding, as proposed by Mares and Kronenberg (1993) for muscovite gouge.

As every grain in gouge would be at all times slightly differently orientated with respect to another (Scruggs and Tullis, 1998; Collettini et al., 2009), the effective stress normal to their (001) planes would be different for each grain, causing the internal stress state over the sample to be non-uniform. Thus, given that normal stress > 100 MPa can potentially inhibit frictional sliding, effective confining pressures would have to be high enough to sustain a normal stress on each grain above the threshold limit, to effectively inhibit frictional behavior in gouge. This may turn out to be unrealistic, given the effective normal stress imposed on gouge in studies like performed by Mariani et al. (2006) and van Diggelen et al. (2010). In general it might be concluded that higher confining pressures are needed to inhibit frictional sliding in gouge, than in single crystals.

5.4) Implications for crustal strength and seismogenesis

To our knowledge, this is the first attempt to include velocity dependence of muscovite single crystals in considerations on the seismogenic zone. It is once more emphasized that for an adequate evaluation more data is required, especially for a wider temperature range given the notion that the seismogenic upper and lower limits are thermally controlled (e.g. Scholz, 2002; Hyndman, 2007).

Muscovite single crystals showed velocity strengthening behavior at 150° and 500°C where strengthening was least pronounced in sample M2 (150°C) that inclined towards velocity neutrality. This is consistent with previous work, as the upper and lower limit of the seismogenic zone and hence the transition to velocity weakening behavior is constrained at ~150-350°C, respectively (e.g. Scholz, 2002; Hyndman, 2007; Marone and Saffer, 2007). Stick-slip behavior has been reported in muscovite gouge at temperatures of 400°-500°C (Mariani et al., 2006; van Diggelen et al., 2010) but was not observed in this study. The above considerations however, have demonstrated the significant difference in mechanical behavior of gouge with respect to

single crystals, so that, for proper analysis of the stability of grain scale sliding, it is again emphasized that obtaining more data at a broader temperature range is indispensible.

The need for a local grain boundary friction coefficient of mica has previously been pointed out for crustal strength modeling studies (e.g. Bos and Spiers, 2002; Niemeijer and Spiers, 2007). Indeed, based on this study input data describing the grain boundary friction coefficient of muscovite may have been overestimated. In their study, Bos and Spiers (2002) proposed a modification of Byerlee's classical crustal strength envelope, where they balanced pressure solution and grain boundary frictional sliding as strength controlling processes. For geologically realistic strain rates (in the order of 10^{-10} s^{-1}) a transition was shown from behavior closely resembling Byerlee's law at shallow depths (0-5 km), to behavior where strength is controlled by grain boundary friction (5-20 km). As the grain boundary friction coefficient determines the slope of strength versus depth line below that transition, a significantly lower friction coefficient as reported in this study may be of strong influence on the total integrated strength of the crust, which in turn controls the strength of earthquakes along muscovite rich faults. Clearly, there is a great need for further systematic experimental work on this.

6) Conclusions

This study aimed to determine the grain scale sliding behavior of muscovite single crystals at dry conditions, high confining pressures (270 – 170 MPa), displacement rates of 0.1 - 10 μm/s and temperatures of 150°, 500° and 600°C. Due to technical difficulties, the data obtained in this study is relatively scarce, and continued research on the topic is called for. Nonetheless, the following conclusions were reached:

1) Pressure stepping experiments have shown that the strength of muscovite single crystals is weakly pressure sensitive. The true coefficient of friction is constrained at ~0.055, or even 0.12, when crystals are sheared in a direction inhibiting dislocation glide, at 500°C. Samples showed only weak temperature dependence where strength slightly dropped with increasing temperature. At elevated temperatures, samples also showed microstructural evidence for kinking, pointing to dislocation glide.

2) Rate-stepping experiments yield stable, velocity strengthening sliding behavior at 150° and 500°C, which is in accordance with current constraints on the seismogenic zone in subduction zones being located in between the 150° and 350°C geotherms.

3) The weak temperature dependence suggests that dislocation motion is not dominant, assuming a relatively high sensitivity of glide to temperature, typical of most crystalline solids as well as muscovite. However, dislocation glide is evidenced in microstructural analysis. The low sensitivity to pressure suggests either frictional slip with a very low friction coefficient, or dominant dislocation glide. Thus, neither dislocation glide, nor friction can be eliminated as mechanisms facilitating deformation.

4) On the basis of the unusually low temperature sensitivity, we infer that muscovite single crystals, stacked upon each other, at the range of temperatures described here, consistently deform through a combination of crystal plastic and frictional processes, where strength is mostly controlled by grain boundary friction.

5) Comparison of muscovite single crystals with muscovite gouge illustrates a pronounced difference in rheology. Single crystals are shown to be a lot weaker than gouge, with a strength that is rate-dependent in a velocity strengthening sense. Additionally, the friction coefficient of muscovite single crystals decreases slightly with temperature, whereas it increases with temperature in gouge. These observations might be of substantial importance in studies on crustal strength and hence on seismogenesis and calls for more attention.

Acknowledgements

First of all, I would like to thank Eimert de Graaff, Peter van Krieken and Gert Kastelein for their technical support and advice. I would also like to thank Colin Peach, for the advice and elevating conversations during experimenting. Chris Spiers is sincerely thanked, who with insightful support, both professionally and personally, not only gave this study more depth, but made it fun as well. Finally, Sabine den Hartog is thanked for the many useful discussions, for thoroughly reviewing this manuscript and for meeting impatience with patience.

Appendix: Jacket Strength

To prevent argon gas from infiltrating the sample pore space and hence producing zero effective normal stress, the sample-piston assembly needs to be jacketed. Thin walled metal jackets (wall thickness of 0.2 and 1 mm for silver and lead tubes, respectively) were used for sample sealing. In addition, the open space between the two pistons needs to be filled up. This is usually done using fillers of the same material as the jackets. Ideally the strength of jackets and fillers is high enough to prevent leakage, but is negligible compared to the shear strength of the sample.

At 150°C, we used lead as preferred jacketing material. Lead is known to have low strength and minimum strain hardening, so that strength corrections are small (~0.290 kN, at T = 150°C and v = 1 μm/s; Frost and Ashby, 1982). Rigid brass tips were soldered at both ends of the jacket pipe to ensure sealing and deformation parallel to the piston-sample interface, i.e. direct shear.

At 600°C, silver seemed the most suitable, weldable jacket material that was commercial readily available, although at ~0.6T_m it was likely to be considerably strong. Therefore, we determined the strength of silver jackets at 600°C in a separate calibration run, using the same direct shear set-up and conditions as imposed on muscovite, but with air-equilibrated (humid) talc as sample. Talc was selected since it is known to be stable up to temperatures of ~750°C (Escartin et al., 2008).

Correction of the strength obtained in this calibration run for the talc strength, however, proved to be difficult, since only a few authors determined the shear strength of humid talc. Horn and Deere (1962) reported a friction coefficient μ of 0.24 at room temperature and pressure, which was confirmed by Scruggs et al. (1993), who reported μ being 0.22 at room temperature and P_c = 25 MPa. In addition, the friction coefficient of air-equilibrated talc is shown to decrease with temperature, to values as low as 0.08-0.1 at 400-600°C (Escartin et al., 2008). A friction coefficient value μ = 0.1 is then likely to be most appropriate for the experimental conditions used in this calibration.

The result of the silver jacket test is shown in figure 11a. The talc strength is here subtracted from the total signal to give the amount of force needed to deform the silver jackets alone. Given μ = 0.1, at P_c = 170 MPa, 1.088 kN is needed to shear humid talc (area = 64 mm^2). This implies that 0.997 kN (17.99 MPa; figure 11b) is needed to deform the silver fillers and jacket, which is in reasonable agreement with the data compiled for silver by Frost and Ashby (1982), (~1.399 kN, at T = 600°C and v = 1 μm/s) given the rather large margin of error that should be considered for the determination of the shear strength of talc. Additionally, figure 11a shows significant strain hardening of the talc sample jacketed with silver. Talc is known to only harden slightly over a relatively large displacement (Moore and Lockner, 2008; personal communication with K.-I. Hirauchi, 2012), so that the hardening observed in figure 11a is likely to be almost entirely an effect of deforming the silver. Besides that, strength in- or decreases in rate-stepping tests (consistently showing velocity strengthening behavior) correspond well with data compiled for silver by Frost and Ashby (1982) and are therefore also likely to be an effect of the jacket, rather than being induced by the sample. Clearly, at $T \leq$ 600°C, a silver jacket- and filler set-up

contributes significantly to the measured strength, indicating the need for alternative jacketing material.

In an attempt to reduce the effect of the jacket strength on the total signal, the muscovite-piston assembly was placed in a silver jacket and annealed aluminum 6082-T6 (Al 6082) alloy fillers were used. Al 6082 has a solidus at 550°C and is known to eutectically melt with silver at 569°C (Lim et al., 1995) making it sufficiently weak at 500°C, whilst remaining in solid form throughout the experiment. The composition of Al 6082 is given in *table 2*.

Table 2: Chemical composition in weight % present of Aluminium 6082-T6 (After Missori and Sili, 2000)

Si	Fe	Cu	Mn	Mg	Zn	Ti	Cr	Al
0.7-1.3	0.0-0.5	0.0-0.1	0.4-1.0	0.6-1.2	0.0-0.2	0.0-0.1	0.0-0.25	Balance

To adequately correct for the strength of these fillers we conducted velocity stepping tests on an Al 6082 cylinder, with a diameter of 10 mm, under the same conditions as experiments M3 and M4, i.e. 170 MPa, 500°C, at displacement rates of 1, 10 and 0.1 μm/s. Before loading, the cylinder was annealed at 520°C for 2 hours in an electric tube oven and subsequently slowly cooled. The result of this test is shown figure 12. After yield the sample shows slight displacement hardening to a displacement of approx. 1.5 mm, where it reaches a steady state strength of 9-9.5 MPa. Velocity stepping clearly shows a rate-dependence of Al 6082 in accordance with Dorn-type plastic deformation.

To summarize, even when tested at temperatures 100°C lower than the silver calibration test, annealed Al 6082 is much weaker and shows less displacement hardening than silver, which makes it more appropriate as a filler material at the experimental conditions used in this study.

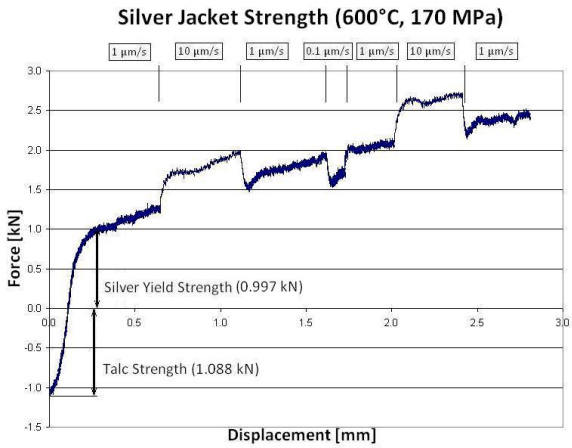

Figure 11a: Results of the silver jacket/filler strength test, after subtraction of talc gouge shear strength. Note the considerable amount of force needed to deform the silver alone, followed by significant shear hardening. The above labels indicate velocity steps.

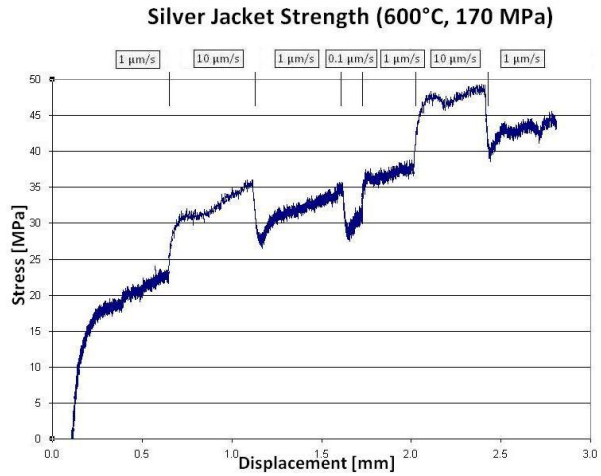

Figure 11b: Plot of normal stress versus displacement, after subtraction of talc gouge shear strength.

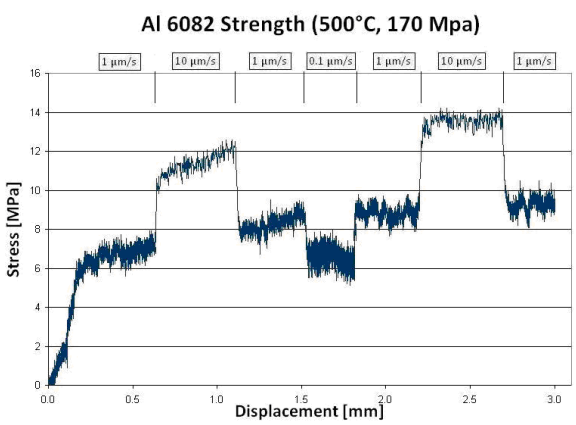

Figure 12: Results of the aluminum alloy 6082 strength test. Note especially the difference in hardening rate compared to that of silver.

References

Aja, S.U. 1997. Comment on 'Formation and stability of endmember illite: I. Solution equilibration experiments at 100 to 250°C and Pv,soln' by D.M. Yates and P.E. Rosenberg. Geochimica et Cosmochimica Acta, vol. 61, No. 20 pp 4455 – 4460.

Appelo, C.A.J. 1979. Layer deformation and crystal energy of micas and related minerals. II. Deformation of the coordination units. American Mineralogist. 64, 424 – 431.

Baños, J.O., Amouric, M., de Fouquet, C. and Baronnet, A. 1983. Interlayering and interlayer slip in biotite as seen by HRTEM. American Mineralogist 68, 754 – 758.

Beeler, N.M., Tullis, T.E., Weeks, J.D. 1994. The roles of time and displacement in the evolution effect in rock friction. Geophysical research letters, vol. 21, 18, 1987-1990.

Beeler, N.M., Tullis, T.E., Weeks, J.D. 1996. Frictional behavior of large displacement experimental faults. J. Geophys. Res., 101, 8697-8715.

Bos, B., and Spiers, C.J. 2001. Experimental investigation into the microstructual and mechanical evolution of phyllosilicate-bearing fault rock under conditions favoring pressure solution. Journal of Structural Geology, 23, 1187-1202.

Bos, B. and Spiers, C.J. 2002. Frictional-viscous flow of phyllosilicate-bearing fault rock: Microphysical model and implications for crustal strength profiles. Journal of geophysical research, vol. 107, no. B2, 2028, 10.101029/2001JB000301.

Collettini, C., Niemeijer, A., Viti, C., Marone, C. 2009. Fault fabric and fault weakness. Nature letters, vol. 462 doi:10.1038/nature08585

Den Hartog, S.A.M., Peach, C.J., De Winter, M.D.A., Spiers, C.J., Shimamoto, T. (2012) Frictional properties of megathrust fault gouges at low sliding velocities: new data on effects of normal stress and temperature. Journal of Structural Geology, doi:10.1016/j.jsg.2011.12.00

Dieterich, J.H. 1978, Time-dependent friction and the mechanics of stick-slip. Pure and Applied Geophysics, 116, 790-806.

Dieterich, J.H. 1979, Modeling of rock friction 1. Experimental results and constitutive equations. Journal of Geophyisical Research, 84, B5, 2161-2168.

Escartin, J., Andreani, M., J., Hirth, G., Evans, B., 2008. Relationships between the microstructural evolution and the rheology of talc at elevated pressure and temperatures. Earth and Planetary Science Letters 268 (2008) 463-475.

Franzini, M. and Schiaffino, L.. 1963. On the crystal structure of biotites. Zeitschrift für Kristallographie, Bd. 119, S. 297 – 309.

Frost and Ashby, 1982 Deformation-Mechanism Maps, The Plasticity and Creep of Metals and Ceramics. Webversion: http://www.thayer.dartmouth.edu/defmech/

Guggenheim, S., Chang, Y-H., Van Groos, K. 1987. Muscovite dehydroxylation: high temperature studies. American Mineralogist, 72, 537-550.

Güven, N. and Burnham, C.W. 1967. The crystal structure of 3T muscovite. Zeitschrift für Kristallopgraphie, Bd. 125, S. 163 – 183.

Hirano, M., Shinjo, K., Kaneko, R., Murata, Y., 1991. Anisotropy of frictional forces in muscovite mica. Physical Review Letters 67, 19.

Horne, H.M. and Deere, D.U. 1962. Frictional characteristics of minerals. Geotechnique 12, 319-335.

Huang, W.L.. and Wyllie, P.J. 1973. Muscovite dehydration and melting in deep crust and subducted oceanic sediments. Earth and planetary science letters 18 133 -136.

Hyndman, R.D. 2007. The seismogenic zone of subduction thrust faults; what we know and don't know. In: Dixon, T.H., Moore, J.C. (Ed.), The seismogenic zone of subduction thrust faults. Columbia University Press, New York, 15-40.

Hyndman, R.D., Yamano, M., Oleskevich, D.A., 1997. The seismogenic zone of subduction thrust faults. The island arc 6, 244-260.

Lachenbruch, A.H. and Sass, J.H. 1980. Heat flow and energetic of the San Andreas fault zone. Journal of Geophysical Research 85, 6185 – 6223.

Lim, S.S., Rossiter, P.L. and Tibballs, J.E. 1995. Assessment of the Al-Ag binary phase diagram. Calphad vol. 19, No. 2, pp. 131-141.

Logan, J.M. and Rauenzahn, K.A. 1987. Frictional dependence of gouge mixtures of quartz and montmorillonite on velocity, composition and fabric. Tectonophysics, 144, 87-108.

Mares, V.M. and Kronenberg, A.K. 1993. Experimental deformation of muscovite. Journal of Structural Geology, 15, 1061-1075.

Mariani, E., Brodie, K.H., Rutter, E.H. 2006. Experimental deformation of muscovite shear zones at high temperature under hydrothermal conditions and the strength of phyllosilicate-bearing faults in nature. Journal of Structural Geology 28, 1569-1587.

Marone , C. and Scholz, C.H. 1988. The Depth of seismic faulting and the upper transition from stable to unstable slip regimes. Geophys. Res. Lett., 15, 621-624.

Marone, C. 1998. Laboratory-derived friction laws and their application to seismic faulting. Annual Review of Earth and Planetary Science, 26, 643-696.

Marone, C. and Saffer, D.M. 2007. Fault friction and the upper Transition from Seismic to Aseismic Faulting. In: Dixon, T.H., Moore, J.C. (Ed.), The seismogenic zone of subduction thrust faults. Columbia University Press, New York, 346-369.

McDonnell,R .D. 1997. Deformation of fine-grained synthetic peridotite under wet conditions.Geol. Ultraiectina no 152, pp 195.

Moore, J.C. and Saffer, D.M. 2001. Updip limit of the seismogenic zone beneath the accretionary prisms of southwest Japan: an effect of diagenetic to low-grade metamorphic processes and increasing effective stress, Geology, 29(2), 183-186

Meike, A. 1989. In situ deformation of micas: A high-voltage electron-microscope study. American Mineralogist, 74, 780-796.

Missori, S. and Sili, A., 2000. Mechanical behaviour of 6082-T6 Aluminium alloy welds. Metallurgical Science and Technology. Vol. 18 (1) pp. 12-18

Moore, D. and Lockner, D.A. 2008. Talc Friction in the temperature range 25°-400°C: relevance for fault-zone weakening.

Moore, D.E. and Lockner, D.A. 2011. Frictional strengths of talc-serpentine and talc-quartz mixtures. Journal of Geophysical Research, 116.

Niemeijer, A.R. and Spiers, C.J. 2005. Influence of phyllosilicates on fault strength in the brittle-ductile transition: insights from rock analogue experiments. Geological Society, London, Special Publications, 245, 303-327.

Niemeijer, A.R. and Spiers, C.J. 2006. Velocity dependence of strength and healing behavior in simulated phyllosilicate-bearing fault gouge. Tectonophysics 427, 231-253.

Niemeijer, A.R. and Spiers, C.J. 2007. A microphysical model for strong velocity weakening in phyllosilicate-bearing fault gouges. Journal of Geophysical Research 112.

Peacock, S.M. and Hyndman, R.D. 1999. Hydrous minerals in the mantle wedge and the maximum depth of subduction thrust earthquakes. Geophysical Research Letters, 26, 2517-2520.

Peierls, R. 1940. The size of a dislocation. Proceedings of the Physical Society of London, 52, 34-37.

Putnis, A. 1992. Introduction to mineral sciences. Cambridge University Press. 194-195.

Radoslovich, E. W. 1960. The structure of muscovite, $KAl_2(Si_3Al)O_{10}(OH)_2$. Acta cryst. 13, 919-932.

Ruina, A., 1983. Slip instability and state variable friction laws. Journal of Geophysical Research, 88, B12, 10359-10370.

Scholz, C.H. 2002. The mechanics of earthquakes and faulting. Cambridge University Press, Cambridge.

Scruggs, V.J., Tullis, T.E., Weeks, J.D., Beeler, N.M., 1993. The role of water in the evolution effect: a comparison between muscovite mica and talc. Eos trans. AGU 74 (43), F590 (Fall Meet. Suppl.)

Scruggs, V.J. and Tullis, T.E. 1998. Correlation between velocity dependence of friction and strain localization in large displacement experiments on feldspar, muscovite and biotite gouge. Tectonophysics 295, 15-40.

Shea, W.T. and Kronenberg, A.K. 1992. Rheology and deformation mechanisms of an isotropic mica schist. Journal of Geophysical Research, 97, 15201-15237.

Shea, W.T. and Kronenberg, A.K. 1993. Strength and anisotropy of foliated rocks with varied mica contents. J. Struct. Geol. 15, 1097-1121.

Silk, E.C.H. and Barnes, R.S. 1961. The observation of dislocations in mica. Acta Metallurgica, vol. 9.

Tembe, S., Lockner, D.A. Wong, T.-F., 2010. Effect of clay content and mineralogy on frictional sliding behavior of simulated gouges: binary and ternary mixtures of quartz, illite and montmorillonite. Journal of Geophysical Research 115, B03416, DOI:10.1029/2009JB006383.

Van Diggelen, E.W.E., De Bresser, J.H.P., Peach, C.J., Spiers, C.J. 2010. High shear strain behavior of synthetic muscovite fault gouges under hydrothermal conditions. Journal of Structural Geology 32 (2010) 1685-1700.

Vrolijk, P. 1990. On the mechanical role of smectite in subduction zones. Geology, 18(8), 703-707.

Wibberley, C.A.J., 1999. Are feldspar-to-mica reactions necessarily reaction-softening processes in fault zones? Journal of Structural Geology 21, 1219 -1227.

Wintsch, C.R.P. and Kronenberg, A.K. 1995. Fluid-rock reaction weakening of fault zones. Journal of Geophysical Research, 100, 13021-13032.

Zoback , M.D., Zoback, M.L., Mount, V.S., Suppe, J., Eaton, J.P., Eaton, J.P., Healy, J.H., Oppenheimer, D., Reasenberg, P., Jones, L., Rayleigh, C.B., Wong, I.G., Scotti, O., Wentworth, C., 1987. New evidence on the state of stress of the San Andreas fault system. Science 238, 1105-1111.